PHYSICAL REVIEW D VOLUME 10, NUMBER 1 1 JULY 1974

Study of the reactions $\bar{K}^0 p \to \Lambda\pi^+$ and $\bar{K}^0 p \to \Sigma^0\pi^+$ from 1 to 12 GeV/c†

R. J. Yamartino,* G. W. Brandenburg, W. B. Johnson, D. W. G. S. Leith,
J. S. Loos,‡ G. J. Luste,§ J. A. J. Matthews, K. Moriyasu,‖
W. M. Smart,¶ and F. C. Winkelmann**
Stanford Linear Accelerator Center, Stanford University, Stanford, California 94305

(Received 18 March 1974)

Cross sections, differential cross sections, and hyperon polarization results are presented for the reactions $\bar{K}^0 p \to \Lambda\pi^+$ and $\bar{K}^0 p \to \Sigma^0\pi^+$ in the momentum interval 1 to 12 GeV/c. Emphasis is placed on the comparison of Λ and Σ channels, and on the momentum dependences of the data. In particular, the Λ polarization data are consistent with being independent of energy above 2 GeV/c; and the slopes of the forward cross sections are found to increase toward the slope values for the line-reversed reactions $\pi p \to K(\Lambda, \Sigma)$ as energy increases.

I. INTRODUCTION

The controversy over the validity of $K^*(890)$-$K^{**}(1420)$ exchange degeneracy[1] (EXD) has traditionally relied heavily on the comparison of the line-reversed reaction pairs

$$\bar{K}N \to \Lambda\pi, \tag{1a}$$

$$\pi N \to \Lambda K \tag{1b}$$

and

$$\bar{K}N \to \Sigma\pi, \tag{2a}$$

$$\pi N \to \Sigma K. \tag{2b}$$

Straightforward comparisons[2-4] of previous experimental data on the reaction pairs (1) and (2) have indicated serious departures from the simple EXD predictions[5-7] and have stressed the need for degeneracy-breaking models and Regge-cut contributions.[8]

We present here a study of the reactions $\bar{K}^0 p \to \Lambda\pi^+$ and $\bar{K}^0 p \to \Sigma^0\pi^+$ in the momentum range from 1 to 12 GeV/c. Emphasis is placed on comparison of the Λ and Σ channels and on momentum dependences in the data. This analysis of K^*-K^{**} exchange degeneracy avoids several of the difficulties intrinsic to the comparison of the line-reversed reaction pairs.

Details of the experiment are discussed in Sec. II. In Sec. III the cross sections, differential cross sections, and polarizations for the $\Lambda\pi^+$ and $\Sigma^0\pi^+$ final states are given along with fitted momentum dependences of the total integrated cross sections. In addition, the quantity $\sigma_{\Sigma\pi}/\sigma_{\Lambda\pi}$ is presented and discussed in terms of final-state interaction differences and the presence of additional exchanges in Λ and Σ channels. The $\sigma_{\Sigma\pi}/\sigma_{\Lambda\pi}$ ratio at $t = t_{\min}$ is then used to extract an f/d ratio consistent with helicity-nonflip dominance.[9-12] Shrinkage of the forward differential cross section is observed, the slopes converging to the slope values of the line-reversed reactions at higher momentum. Effective trajectories for the reactions are found to be consistent with a linear trajectory passing through $K^*(890)$ and $K^{**}(1420)$, while the lack of momentum dependence in the Λ polarization is interpreted as evidence for the equality of the K^*-K^{**} trajectory functions. Further discussion of theoretical models is given in Sec. IV, with a summary of conclusions contained in Sec. V.

II. EXPERIMENTAL DETAILS

A. Bubble-chamber exposure and the K_L^0 beam

The data were obtained by exposing the Stanford Linear Accelerator Center (SLAC) 40-in. (1-m) hydrogen bubble chamber to a neutral beam of K_L^0 mesons. The analysis of reactions (1a) and (2a) has been carried out using approximately one million photographs representing ~40 events/μb. Final samples of 2512 events for the reaction $\bar{K}^0 p \to \Lambda\pi^+$ and 1165 events for $\bar{K}^0 p \to \Sigma^0\pi^+$ were obtained.

The K_L^0 beam was produced by impinging a high-energy electron beam onto a beryllium target 56 m upstream of the bubble chamber, and yielded approximately 25 K_L^0 per picture. The K_L^0 momentum spectrum, shown in Fig. 1, peaks near 4 GeV/c and extends to 12 GeV/c. Details on the construction of the beam line and the determination of the K_L^0 momentum spectrum are discussed elsewhere.[13]

B. Scanning and measuring procedures

The entire film sample was scanned for vee events. Events for the reactions considered here belong to the "1-prong-vee" category, whereas decays of the K_L^0 beam belong to the "unassociated vee" category. From a second scan of 10% of the

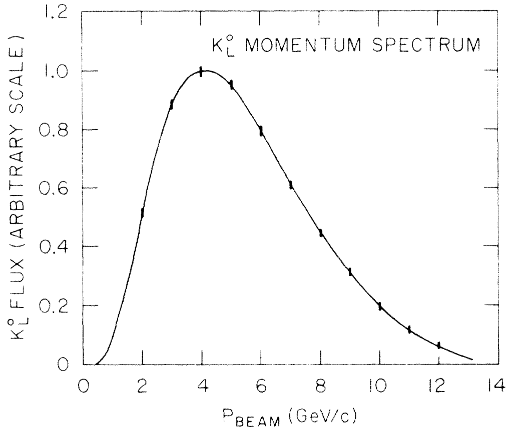

FIG. 1. K_L^0 beam momentum spectrum shape.

film, the scanning efficiencies were determined to be (92 ± 2)% for both categories. Thus the scanning efficiency corrections cancel when 1-prong-vee cross sections are computed. Measurements were done both on film plane digitizers and on the SLAC spiral reader with no apparent differences in accuracy. Especially difficult events were remeasured on the film plane machines. The programs TVGP and SQUAW were used for spatial reconstruction and kinematic fitting.

Care was taken to ensure the correct association of vees to interactions. In cases of doubtful association of a vee, the scanners were instructed to assign the vee to *n*-prong-vee categories rather than to the unassociated vee category. After measurement of all *n*-prong-vee events, those vees which were really K_L^0 beam decays were identified and reassigned (this amounted to an 8% increase in the number of K_L^0 beam decays). Similarly, a fraction of the events measured as unassociated vees appeared to be K_S^0 or Λ decays. These vees were then reexamined at the scan table to search for an associated interaction. This procedure increased the sample of 1-prong-vee events by 5%.

C. Event selection and biases

The events in the $\Lambda\pi^+$ final state have six kinematic constraints (three each for the interaction vertex and the decay vertex), while events in the $\Sigma^0\pi^+$ final state have four constraints. Contamination from kinematically ambiguous hypotheses involving a K_S^0 is less than 2%; however, ambiguities exist with other hypotheses involving a Λ, and these will be discussed in Sec. II D after dealing with biases in Λ detection.

Asymmetries were observed both in the laboratory azimuthal distribution of the Λ decay about its direction of flight and in the helicity cosine distribution of the proton in the Λ decay. Losses in these otherwise flat distributions are strongly correlated with one another and are understood in terms of low-vee-detection processing efficiencies for short and/or steeply dipping protons. As shown in Table I(a), these losses are strongly dependent on Λ momentum, rising from ~7% for $P_\Lambda > 400$ MeV/*c* to ~20% for $195 < P_\Lambda < 400$ MeV/*c* (this corresponds to $0.0 \leq -t \leq 0.1$ GeV^2 for $\bar{K}^0 p \to \Lambda\pi^+$). Below $P_\Lambda \sim 195$ MeV/*c* these losses climb sharply, and these small-*t* data have consequently been excluded from the studies of the differential cross sections.

A reduced interaction volume was imposed on the events to ensure uniform detection efficiency of the Λ decays, to allow a minimum of ~15 cm for measurement of tracks from the decay vertex, and to guarantee a Λ decay region at least ~5 cm in length. The scanning efficiency discussed in the previous section was determined for events with Λ flight paths (l_Λ) between 2 cm and approximately 20 cm. The efficiency was found to be uniform in this interval; however, for both shorter and longer l_Λ a slowly falling efficiency was found. The average efficiencies, normalized to the central region of l_Λ, are given as a function of l_Λ in Table I(b). In addition to being corrected for these efficiencies, the events were compensated for the effect of the finite fiducial volume by weighting with the factor

$$W = [\exp(-L_{\min}/\lambda) - \exp(-D/\lambda)]^{-1},$$

where D is the distance along the Λ flight path to

TABLE I. Efficiencies for Λ detection.

(a) Azimuthal and slow-proton losses

P_Λ (MeV/*c*)	$-t$ (GeV^2) for $\bar{K}^0 p \to \Lambda\pi^+$	Efficiency
< 195	< 0	0.46
195 – 400	0.0 – 0.1	0.81
> 400	> 0.1	0.93

(b) Scanning efficiency versus Λ decay length

Decay length l_Λ (cm)	Normalized scanning efficiency
0.3 – 0.5	0.84
0.5 – 1.0	0.91
1.0 – 2.0	0.94
2.0 – 18.7	1.00
18.7 – 30.0	$1 - 0.0187(l_\Lambda - 18.7)$

(c) Other correction factors

1-prong-*V* improperly scanned as K_L^0 beam decays	1.05
1-prong-*V*/beam decay relative scanning-processing eff.	(No correction)[a]
Unobserved Λ decay modes	1.56
Confidence level cut at 1%	1.01
Σ^0 mass cut	1.05
Loss of Σ^0 data from residual Λ, Σ^0 ambiguities	1.03
Contamination of Σ^0 data from Λ channels	(> 0.98)[a]
Contamination of Λ data by Σ^0 events	(> 0.99)[a]

[a] Corrections in parentheses have been neglected.

the edge of the fiducial volume and λ is the mean decay length[14] for the Λ in question. The minimum l_Λ accepted, $L_{\min}$, was taken to be 0.3 cm for events with $p_\Lambda < 2$ GeV/c and 0.5 cm for larger p_Λ. Events with $l_\Lambda > 30$ cm were rejected as well; thus the maximum value of D was 30 cm.

For further details on the event selection and weighting procedure see Ref. 15.

D. Λ and Σ^0 signal quality

With the imposition of a 1% minimum confidence-level cut on accepted events, contamination from final states containing a K^0_S was reduced to a negligible level; however, nearly 80% of events with a good 6-C $\Lambda\pi^+$ fit also had an accompanying 4-C $\Sigma^0\pi^+$ fit with comparable confidence level. This results from the energy of the incident $\bar{K}^0$ being umeasured. Thus a low-momentum γ ray is easily inserted along the beam direction, and a legitimate $\Lambda\pi^+$ event can nearly always obtain a fit to the $\Sigma^0\pi^+$ hypothesis.

In order to study this problem, the zero-constraint[16] hypothesis $\bar{K}^0p \to \Lambda\gamma\pi^+$ was tried for all events. The resulting $\Lambda\gamma$ invariant-mass plot (Fig. 2) for Λ, Σ^0 ambiguities suggests that most of the ambiguities indeed belong to the more highly constrained $\Lambda\pi^+$ category. Fortunately, the electromagnetic decay of Σ^0 into $\Lambda\gamma$ gives rise to an isotropic γ-ray distribution in the Σ^0 rest frame, and use of this fact allows an improved separation of the two final states. In Fig. 3 we have plotted the ambiguous events with respect to $\hat{\gamma}\cdot\hat{\bar{K}}^0$ and $\hat{\gamma}\cdot\hat{n}$ in the $\Lambda\gamma$ rest system, where $\hat{n}$ is the normal to the over-all production plane. The concentration of events at $\hat{\gamma}\cdot\hat{\bar{K}}^0 \approx 1$ must be primarily real $\Lambda\pi^+$ events, since the number of $\Sigma^0\pi^+$ events expected there on the basis of isotropy is much smaller. However, studies of the kinematic confidence levels for events in the remainder of the plot indicate that they are predominantly real $\Sigma^0\pi^+$ events. Therefore, the events outside the "double-rectangle" region[17] shown in Fig. 3 are included in the $\Sigma^0\pi^+$ sample, while those inside are assumed to be $\Lambda\pi^+$ events. The shape of this dividing boundary has been chosen so as to maximize the number of Σ^0 fits, consistent with preservation of an isotropic γ-ray distribution (Fig. 4)

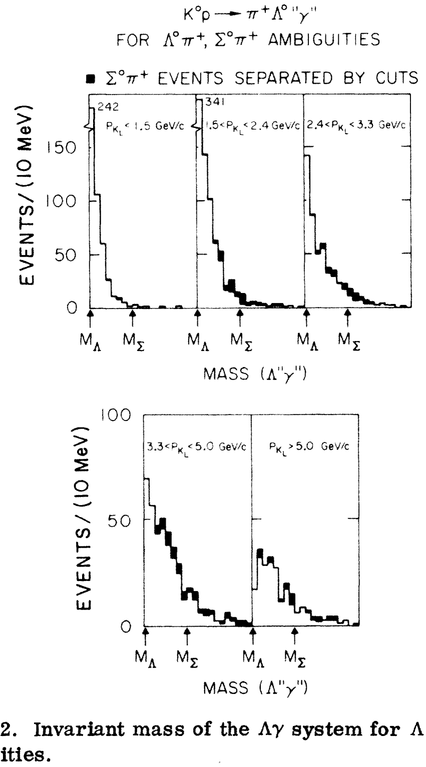

FIG. 2. Invariant mass of the $\Lambda\gamma$ system for Λ, Σ^0 ambiguities.

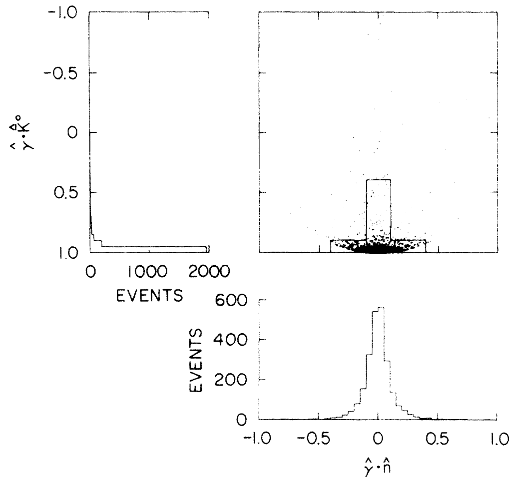

FIG. 3. Distribution of Λ, Σ^0 ambiguities with respect to $\hat{\gamma}\cdot\hat{\bar{K}}^0$ and $\hat{\gamma}\cdot\hat{n}$ in the Σ^0 rest frame.

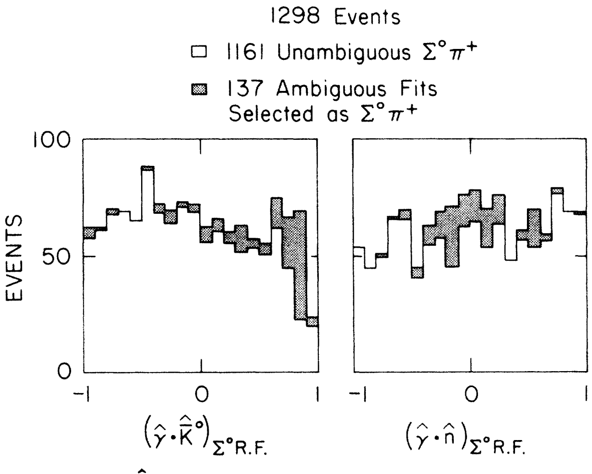

FIG. 4. $\hat{\gamma}\cdot\hat{\bar{K}}^0$ and $\hat{\gamma}\cdot\hat{n}$ distributions for accepted Σ^0 events in the Σ^0 rest frame.

for the entire Σ^0 sample.

The events obtained from this separation of ambiguities constitute a ~12% addition to the unambiguous $\Sigma^0\pi^+$ events. Their $\Lambda\gamma$ mass distribution is shown by the shaded bins in Fig. 2. They are again seen as the shaded contribution to Fig. 4, which depicts the $\hat{\gamma}\cdot\hat{\bar{K}}^0$ and $\hat{\gamma}\cdot\hat{n}$ distributions for all $\Sigma^0\pi^+$ fits. The inclusion of these events clearly improves the uniformity of the $\hat{\gamma}\cdot\hat{\bar{K}}^0$ distribution. However, the remaining dip near $\hat{\gamma}\cdot\hat{\bar{K}}^0 = 1$ represents lost $\Sigma^0\pi^+$ events which are ambiguous and fall in the double rectangle of Fig. 3. They are compensated for by an over-all correction factor of 1.03. Conversely, these $\Sigma^0\pi^+$ events contaminate the $\Lambda\pi^+$ sample at approximately the 1% level. We estimate that the contamination of real $\Lambda\pi^+$ events in the $\Sigma^0\pi^+$ sample is less than a few percent.

Another potential threat to the purity of the Σ^0 sample comes from the possible influx of "$\Lambda\pi^+$ neutrals" events. Allowing the γ ray to represent all missing neutrals, one observes in the $\Lambda\gamma$ mass distribution with $\Lambda\pi^+$ events removed (Fig. 5) a clean Σ^0 peak, well separated from the high-mass continuum background. Although the Σ^0 broadens somewhat at higher beam momenta, the available phase space for non-Σ^0 events conveniently spreads out, leaving the Σ^0 purity rather constant as a function of momentum. The $\Lambda\pi^+\pi^0$ channel appears to be the chief contamination of the high-mass side of the Σ^0, its effects seemingly more pronounced at large momentum transfers, where low statistics inhibit a more detailed analysis. However, the mass resolution is good enough to ensure against any $Y_1(1385)\to\Lambda\pi^0$ resonance contribution to the Σ^0 signal.

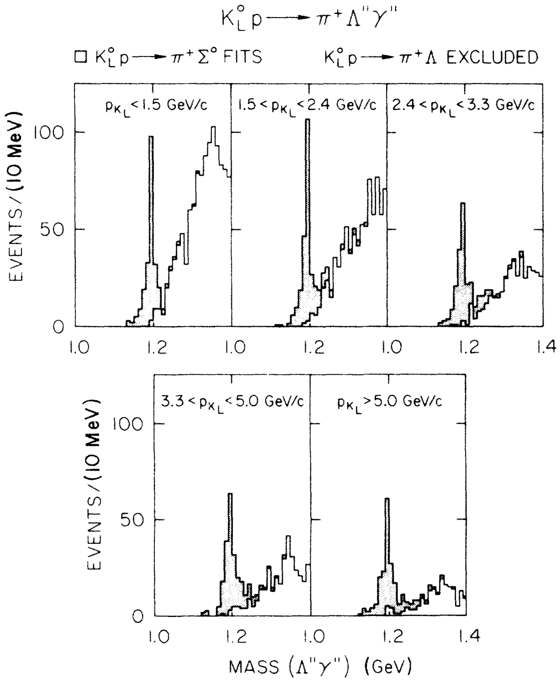

FIG. 5. Invariant mass of the $\Lambda\gamma$ system; $\bar{K}^0p \to \Lambda\pi^+$ events are excluded. The shaded events are in the channel $\bar{K}^0p \to \Sigma^0\pi^+$.

A high-mass cutoff for the Σ^0 was determined by first assuming the low-mass side of the Σ^0 to be uncontaminated, then computing a width, $\Delta M \sim 32.5$ MeV, which included 90% of the events below the central value. The Σ^0 upper-mass cutoff was then set at $M_\Sigma + \Delta M \sim 1225$ MeV. The cross sections have been increased by 5% to compensate for this cut. Then assuming symmetry of the Σ^0 about its central mass value, contamination of the high-mass side was estimated to be less than a few percent; consequently no additional correction has been made.

The various correction factors are summarized in Table I(c). Exclusive of the $\Lambda\to p\pi^-$ branching ratio factor, the average event weight was 1.44 for the $\Lambda\pi^+$ data and 1.55 for the $\Sigma^0\pi^+$ data.

III. RESULTS

A. Cross sections versus beam momentum

Cross sections as a function of incident $\bar{K}^0$ momentum are given in Table II for the reactions $\bar{K}^0p\to\Lambda\pi^+$ and $\bar{K}^0p\to\Sigma^0\pi^+$. The cross sections have been corrected for the neutral decay mode of the Λ as well as for scanning biases and losses due to decays outside the active scanning volume (see Sec. II). Errors on the cross sections include statistical uncertainties, the effects of the dispersion in event weights, and uncertainties in the shape of the beam momentum distribution as indicated by the error bars in Fig. 1. The over-all normalization of the data was determined from a measurement of the K^0_L flux for ~25% of the film. Systematic uncertainty on the normalization was determined to be $\leq 15\%$.[13] This additional uncertainty has not been folded into quoted cross-section errors.

The cross sections are displayed in Figs. 6 and 7 along with representative data from other experiments.[18-20] The $\bar{K}^0p\to\Lambda\pi^+$ data are compared directly to data on $K^-n\to\Lambda\pi^-$, while cross sections for $K^-p\to\Lambda\pi^0$ must be multiplied by 2 since the initial state is half isospin one. In Fig. 6 the $\bar{K}^0p\to\Sigma^0\pi^+$ data are to be compared directly with the data for $K^-n\to\Sigma^0\pi^0$; however, comparison to $K^-p\to\Sigma^+\pi^-$ data is not straightforward. From isospin considerations the amplitudes for the three processes may be written as[19b]

TABLE II. Total cross sections.

p_{beam} (GeV/c)	Observed no. of events	$\sigma(\bar{K}^0p \to \Lambda\pi^+)$	p_{beam} (GeV/c)	Observed no. of events	$\sigma(\bar{K}^0p \to \Sigma^0\pi^+)$
0.6 – 0.8	52	4.51 ± 0.69 mb	0.6–0.8	26	2.32 ± 0.49 mb
0.8 – 1.0	105	4.68 ± 0.52	0.8–1.0	41	1.86 ± 0.30
1.0 – 1.2	146	3.77 ± 0.34	1.0–1.2	44	1.16 ± 0.18
1.2 – 1.4	154	2.58 ± 0.22	1.2–1.4	43	777 ± 123 μb
1.4 – 1.6	186	2.36 ± 0.18	1.4–1.8	113	661 ± 65
1.6 – 1.8	185	1.85 ± 0.14	1.8–2.2	102	413 ± 43
1.8 – 2.0	157	1.28 ± 0.11	2.2–2.6	91	264 ± 28
2.0 – 2.2	143	959 ± 84 μb	2.6–3.0	98	250 ± 27
2.2 – 2.4	139	776 ± 68	3.0–3.5	98	154 ± 16
2.4 – 2.6	143	724 ± 63	3.5–4.0	80	123 ± 15
2.6 – 2.8	123	570 ± 53	4.0–4.5	75	109 ± 13
2.8 – 3.0	98	440 ± 46	4.5–5.0	50	75 ± 11
3.0 – 3.2	87	338 ± 38	5.0–6.0	84	65 ± 7
3.2 – 3.4	80	292 ± 34	6.0–7.0	52	50 ± 7
3.4 – 3.8	135	236 ± 21	7.0–8.0	34	41 ± 7
3.8 – 4.2	123	216 ± 21	8.0–10.0	29	30 ± 6
4.2 – 4.6	83	141 ± 16	10.0–12.0	5	13 ± 7
4.6 – 5.0	63	104 ± 14			
5.0 – 5.5	83	123 ± 14			
5.5 – 6.0	64	95 ± 12			
6.0 – 7.0	77	68 ± 8			
7.0 – 8.0	41	47 ± 8			
8.0 – 10.0	35	30 ± 5			
10.0 – 12.0	10	26 ± 9			

$$A(\bar{K}^0p \to \Sigma^0\pi^+) = A(K^-n \to \Sigma^0\pi^-)$$

$$= \frac{1}{\sqrt{2}}[A(K^-p \to \Sigma^+\pi^-) - A(K^-p \to \Sigma^-\pi^+)]\,.$$

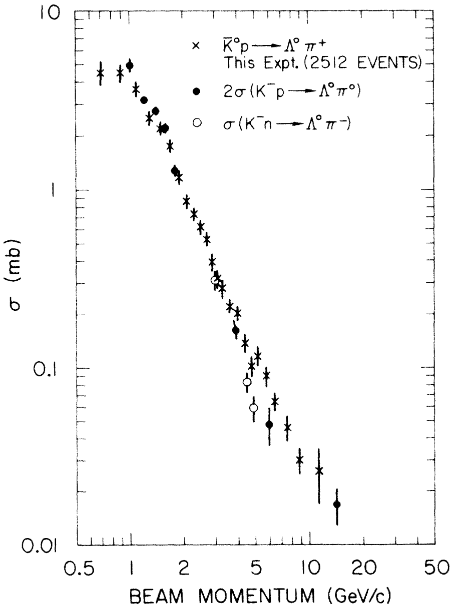

FIG. 6. Cross sections versus incident momentum for $\bar{K}^0p \to \Lambda\pi^+$. Other data are from Refs. 18 and 19.

If t-channel exchanges with isospin $\frac{3}{2}$ could be neglected, then $A(K^-p \to \Sigma^-\pi^+)$ would vanish, and the natural comparison would be to $\frac{1}{2}\sigma(K^-p \to \Sigma^+\pi^-)$ as given. However, data on K^-p-induced reactions[21] indicate that the quantity

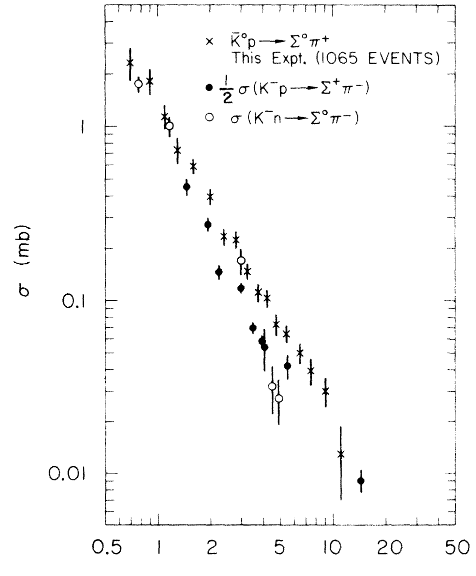

FIG. 7. Cross sections versus incident momentum for $\bar{K}^0p \to \Sigma^0\pi^+$. Other data are from Refs. 18 and 20.

TABLE III. Fits to $\sigma = AP_{\text{beam}}^{\;n}$.

Reaction	P_{beam} interval (GeV/c)	A (mb)	n	Reference
$\bar{K}^0 p \to \Lambda\pi^+$	1.8–12.0	5.9 ± 0.5	-2.44 ± 0.07	This exp.
	1.8–5.0	7.0 ± 0.8	-2.62 ± 0.10	This exp.
	5.0–12.0	4.3 ± 0.3	-2.21 ± 0.19	This exp.
$K^- p \to \Lambda\pi^0$	1.5–6.0	5.20 ± 0.28	-3.30 ± 0.10	Ref. 21
$\pi^- p \to \Lambda K^0$	2.0–6.0	0.79 ± 0.14	-1.93 ± 0.17	Ref. 22
$\bar{K}^0 p \to \Sigma^0\pi^+$	1.8–12.0	1.3 ± 0.2	-1.78 ± 0.09	This exp.
	1.8–5.0	1.4 ± 0.2	-1.85 ± 0.15	This exp.
	5.0–12.0	1.3 ± 0.7	-1.74 ± 0.31	This exp.
$K^- p \to \Sigma^+\pi^-$	1.0–5.5	1.86 ± 0.04	-2.00 ± 0.07	Ref. 21
$\pi^- p \to \Sigma^0 K^0$	2.0–6.0	0.46 ± 0.13	-1.82 ± 0.28	Ref. 22

$$|R| = [\sigma(K^- p \to \Sigma^-\pi^+)/\sigma(K^- p \to \Sigma^+\pi^-)]^{1/2}$$

decreases from $\sim\frac{1}{2}$ at 2 GeV/c to $\sim\frac{1}{4}$ near 5 GeV/c. Observing in Fig. 6 that $\frac{1}{2}\sigma(K^- p \to \Sigma^+\pi^-)$ is consistently only about two-thirds of $\sigma(\bar{K}^0 p \to \Sigma^0\pi^+)$, a value of $|R| \sim 0.2$ is suggested, in agreement with the range of $|R|$ obtained from $K^- p$ data.

The data for both the $\Lambda\pi^+$ and $\Sigma^0\pi^+$ cross sections have been fitted to the power law $\sigma = AP_{\text{beam}}^{\;n}$, and the result given in Table III along with the A and n coefficients for some related processes.[21,22] One observes the $\bar{K}$-induced cross sections to be considerably larger but falling more rapidly than their companion line-reversed π cross sections over the momentum intervals considered.

The low-energy data are replotted in Fig. 8, where $\sigma/4\pi k_i k_f$ is displayed as a function of center-of-mass energy.[23] These data as well as the cross sections, σ, are recorded in Table IV. In the case of $\bar{K}^0 p \to \Lambda\pi^+$, the interval $1.8 \leq P_{\text{beam}} \leq 5.0$ GeV/c includes the $\Sigma(2250)$ and $\Sigma(2455)$ enhancements as well as possible structure near 3 GeV. It is therefore not surprising to find a steeper P_{beam} dependence ($n = -2.62 \pm 0.10$) in this region than is usually associated with strange-meson exchange.[24] However, in the higher momentum interval $5 \leq P_{\text{beam}} \leq 12$ GeV/c, where meson exchange might be expected to dominate, we find no significant difference, $n_\Sigma - n_\Lambda = 0.47 \pm 0.36$, in the momentum dependences of the $\Lambda\pi^+$ and $\Sigma^0\pi^+$ cross sections.

B. $\sigma_{\Sigma\pi}/\sigma_{\Lambda\pi}$ versus beam momentum

To compare directly the Σ^0 and Λ cross sections, the ratio $\sigma(\bar{K}^0 p \to \Sigma^0\pi^+)/\sigma(\bar{K}^0 p \to \Lambda\pi^+)$ is tabulated in Table V and plotted in Fig. 9. This cross-section ratio is insensitive to over-all normalization uncertainty as well as errors in the spectral shape; hence, the quoted errors reflect only statistical uncertainty.[25] Above 1 GeV/c we see a steady rise of the ratio from ~0.3 at 1 GeV/c to ~0.6 near 6 GeV/c followed by a possible leveling off of the ratio to an asymptotic value of ~0.8 in the 6–12-GeV/c region. We note that the ratio 0.79 ± 0.10 in the 6–12-GeV/c region compares favorably with the ratios 0.79 ± 0.02, 0.76 ± 0.02, and 0.75 ± 0.11 of Foley *et al.*,[26(e)] obtained at 8, 10.7, and 15.7 GeV/c, respectively, for the line-reversed reactions $\pi^- p \to K^0(\Lambda, \Sigma^0)$.

The rapid rise in $\sigma_{\Sigma\pi}/\sigma_{\Lambda\pi}$ over the 1–6-GeV/c beam momentum interval is apparently the result of two effects. First, in the region $1.5 < P_{\text{beam}} < 3.0$ GeV/c the $\Lambda\pi^+$ channel appears to couple more strongly to $I = 1$ s-channel resonances than the $\Sigma^0\pi^+$ channel. Equivalently we observe that in the backward scattering region baryon exchange is considerably more important in $\Lambda\pi^+$ than in $\Sigma^0\pi^+$ for momenta ≤ 3 GeV/c (see Sec. IIIC). Second, we note that the $\Lambda\pi^+$ differential cross section in the very forward direction ($0.00 \leq -t < 0.05$ GeV^2) appears to flatten as the energy increases, whereas the $\Sigma^0\pi^+$ data show no signs of such a trend. Differences in final-state interac-

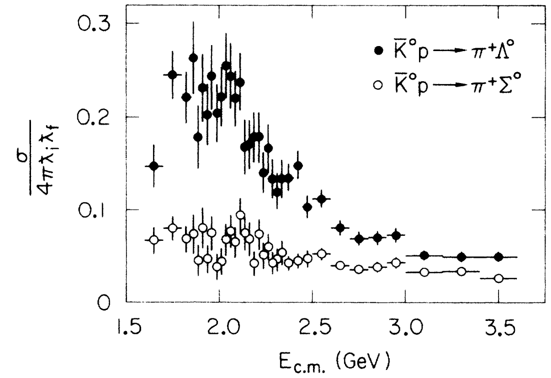

FIG. 8. $\sigma/4\pi k_i k_f$ versus center-of-mass energy for $\bar{K}^0 p \to \Lambda\pi^+$ (solid points) and $\bar{K}^0 p \to \Sigma^0\pi^+$ (open points).

TABLE IV. Cross sections for $\bar{K}^0p \to \Lambda\pi^+$ and $\bar{K}^0p \to \Sigma^0\pi^+$ in the resonance region.

$E_{\text{c.m.}}$ (GeV/c)	$K^0p \to \Lambda\pi^+$		$K^0p \to \Sigma^0\pi^+$	
	σ (μb)	$10^3\sigma/4\pi ƛ_i ƛ_f$	σ (μb)	$10^3\sigma/4\pi ƛ_i ƛ_f$
1.60–1.70	4229 ± 647	147 ± 22	2131 ± 454	67.2 ± 14.2
1.70–1.80	4844 ± 506	245 ± 25	1804 ± 287	80.0 ± 12.6
1.80–1.85	3581 ± 453	221 ± 28	1211 ± 256	68.2 ± 14.4
1.85–1.875	3819 ± 567	263 ± 39	1172 ± 328	74.0 ± 20.7
1.875–1.90	2438 ± 458	179 ± 33	680 ± 242	45.5 ± 16.2
1.90–1.925	2974 ± 463	231 ± 36	1115 ± 308	80.2 ± 22.1
1.925–1.95	2450 ± 388	202 ± 32	604 ± 192	46.8 ± 14.9
1.95–1.975	2786 ± 389	243 ± 34	925 ± 226	74.8 ± 18.3
1.975–2.00	2219 ± 338	204 ± 31	447 ± 162	38.6 ± 14.0
2.00–2.025	2290 ± 323	221 ± 31	489 ± 156	44.2 ± 14.1
2.025–2.05	2507 ± 343	255 ± 35	715 ± 181	67.8 ± 17.2
2.05–2.075	2289 ± 326	244 ± 35	771 ± 178	77.2 ± 17.8
2.075–2.10	1964 ± 265	220 ± 30	620 ± 156	64.9 ± 16.4
2.10–2.125	2039 ± 265	238 ± 31	853 ± 183	94.0 ± 20.2
2.125–2.15	1381 ± 237	168 ± 29	652 ± 148	75.3 ± 17.1
2.15–2.175	1340 ± 205	170 ± 26	567 ± 148	68.4 ± 17.9
2.175–2.20	1347 ± 199	178 ± 26	337 ± 102	42.4 ± 12.9
2.20–2.225	1294 ± 191	178 ± 26	561 ± 124	73.7 ± 16.3
2.225–2.25	984 ± 150	141 ± 22	374 ± 104	50.8 ± 14.1
2.25–2.275	1120 ± 171	167 ± 26	425 ± 98	60.2 ± 13.9
2.275–2.30	868 ± 134	134 ± 21	290 ± 81	42.5 ± 11.9
2.30–2.325	752 ± 122	120 ± 20	302 ± 78	46.1 ± 12.0
2.325–2.35	807 ± 123	134 ± 20	341 ± 83	53.7 ± 13.1
2.35–2.40	772 ± 83	135 ± 15	250 ± 48	42.1 ± 8.0
2.40–2.45	799 ± 80	149 ± 15	252 ± 47	45.1 ± 8.3
2.45–2.50	522 ± 63	104 ± 13	247 ± 50	47.3 ± 9.6
2.50–2.60	521 ± 43	113 ± 9	250 ± 31	52.4 ± 6.4
2.60–2.70	334 ± 32	81.3 ± 7.8	171 ± 23	40.0 ± 5.3
2.70–2.80	256 ± 26	69.1 ± 7.0	136 ± 19	35.6 ± 5.1
2.80–2.90	235 ± 24	70.1 ± 7.1	130 ± 19	38.1 ± 5.6
2.90–3.00	221 ± 23	72.7 ± 7.6	134 ± 18	42.8 ± 5.9
3.00–3.20	137 ± 13	50.9 ± 4.8	87.7 ± 10.3	32.1 ± 3.8
3.20–3.40	113 ± 11	49.3 ± 5.0	78.0 ± 9.6	33.5 ± 4.1
3.40–3.60	97.2 ± 10.5	49.4 ± 5.4	51.3 ± 7.8	25.7 ± 3.9

tions or different helicity-flip/helicity-nonflip coupling strengths are possible sources of these small-t effects.

Hence, elimination of the very forward region $-t \le 0.05$ GeV^2, as well as the region where nonperipheral contributions begin to enter, should

TABLE V. $\sigma(\bar{K}^0p \to \Sigma^0\pi^+)/\sigma(\bar{K}^0p \to \Lambda\pi^+)$

p_{beam} (GeV/c)	All t	$0.05 \le -t \le 0.4$ GeV^2
0.5–1.0	0.59 ± 0.10	0.89 ± 0.24
1.0–1.5	0.29 ± 0.03	0.32 ± 0.06
1.5–2.0	0.36 ± 0.04	0.51 ± 0.10
2.0–2.5	0.35 ± 0.04	0.50 ± 0.09
2.5–3.0	0.46 ± 0.05	0.49 ± 0.09
3.0–3.5	0.51 ± 0.06	0.45 ± 0.08
3.5–4.0	0.55 ± 0.08	0.45 ± 0.10
4.0–5.0	0.64 ± 0.07	0.67 ± 0.11
5.0–6.0	0.60 ± 0.08	0.51 ± 0.10
6.0–8.0	0.79 ± 0.11	0.57 ± 0.11
8.0–12.0	0.77 ± 0.21	0.64 ± 0.20

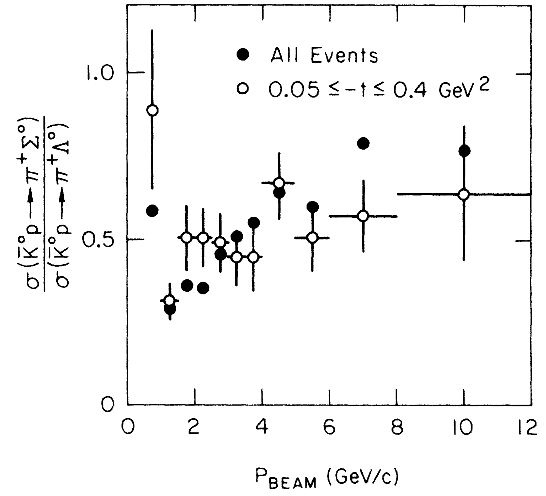

FIG. 9. The ratio $\sigma_{\Sigma\pi}/\sigma_{\Lambda\pi}$ versus incident momentum for all momentum transfers (solid points), and for $0.05 \le -t \le 0.4$ GeV^2 (open points).

yield a more constant value for $\sigma_{\Sigma\pi}/\sigma_{\Lambda\pi}$. Indeed, Table V and Fig. 9 (open data points) show the $\sigma_{\Sigma\pi}/\sigma_{\Lambda\pi}$ ratios for $0.05 \leqslant -t \leqslant 0.4$ GeV^2 to be relatively energy-independent above 1.5 GeV/*c*, as might be expected from a simple picture involving K^* and K^{**} Regge exchanges. An average value of $\sigma_{\Sigma\pi}/\sigma_{\Lambda\pi} = 0.513 \pm 0.017$ is obtained for these data in the interval $1.5 \leqslant P_{\text{beam}} \leqslant 12$ GeV/*c*.

We also note that some of the rise in $\sigma_{\Sigma\pi}/\sigma_{\Lambda\pi}$ may possibly be the result of phase-space and angular-momentum-barrier differences arising from the inequality of the Λ and Σ^0 masses. Trilling[27] has pointed out that a factor $(p_i/p_f)^{2l+1}$ must be included before making comparisons between reactions involving unequal mass initial and final states. A relative rise of ~25% in $\sigma_{\Sigma\pi}/\sigma_{\Lambda\pi}$ between 1.5 and 5 GeV/*c* is accommodated by this factor.

C. Differential cross sections

The data for both final states are presented as a function of $\cos\theta$ in Table VI and Figs. 10 and 11. In addition, the forward scattering data are given as a function of momentum transfer, *t*, in Table VII and Figs. 12 and 13. All data are presented in five momentum intervals between 1.5 and 12 GeV/*c*. As with the total cross sections all errors have been folded in, excepting the over-all normalization uncertainty of ⩽15%.

Both Λ and Σ reactions are characterized by a sharp forward peak, and a backward peaking for the data with $P_{\text{beam}} > 3.5$ GeV/*c*. The cross section at 90° appears to fall off faster with increasing momenta than in any other region of $\cos\theta$, as has been discussed elsewhere.[28]

Fitting the data in the interval $-0.7 \geqslant \cos\theta \geqslant -1$ with the power-law dependence, $\sigma_{\text{back}} = Ap^n$, yields $(765 \pm 246\ \mu\text{b}) \times P_{\text{beam}}^{-3.2\pm0.3}$ for $\Lambda\pi^+$ and $(155 \pm 70\ \mu\text{b}) \times P_{\text{beam}}^{-2.1\pm0.4}$ for $\Sigma^0\pi^+$ for momenta > 1.5 GeV/*c*. Thus the ratio of Λ to Σ backward cross sections decreases rapidly with momentum, with the exponent $n_\Lambda - n_\Sigma = -1.1 \pm 0.5$. Only N exchange contributes to the $\Lambda\pi^+$ backward cross section, while both N and Δ exchanges can contribute to the $\Sigma^0\pi^+$ channel. Thus the difference in momentum dependences for the Λ and Σ data suggests that Δ exchange dominates the $\Sigma^0\pi^+$ channel.[29] In fact, we note that the difference in P_{beam} dependence, $n_\Lambda - n_\Sigma$, is consistent with the difference in the Regge intercepts $2[\alpha_{N_\alpha}(0) - \alpha_{\Delta_\delta}(0)] = -1.1$.[30]

Considering the data as a function of momentum transfer *t* we see strong forward peaking in both channels at all momenta. Both reactions also have

TABLE VI. Differential cross sections (in μb/steradian).

	Beam momentum interval (GeV/*c*)				
$\cos\theta$	1.5–2.5	2.5–3.5	3.5–5	5–8	8–12
		$\bar{K}^0 p \to \Lambda\pi^+$			
−1.0 to −0.9	52 ± 13	11 ± 5	5.2 ± 1.1	0.54 ± 0.24	$0.20^{+0.30}_{-0.14}$
−0.9 to −0.75	56 ± 11	8.6 ± 3.1			
−0.75 to −0.5	47 ± 8	23 ± 4			
−0.5 to −0.2	101 ± 10	15 ± 3	1.9 ± 0.4	0.23 ± 0.12	⋯
−0.2 to 0.2	85 ± 8	13 ± 2			
0.2 to 0.5	91 ± 9	24 ± 3			
0.5 to 0.7	107 ± 11	23 ± 4	6.2 ± 1.4	0.78 ± 0.39	⋯
0.7 to 0.8	106 ± 15	46 ± 8	12 ± 3	3.3 ± 1.1	⋯
0.8 to 0.9	175 ± 20	110 ± 12	50 ± 6	12 ± 2	$2.7^{+4.0}_{-1.9}$
0.9 to 0.95	341 ± 44	157 ± 20	105 ± 12	33 ± 5	7.3 ± 3.5
0.95 to 1.0	442 ± 65	250 ± 27	197 ± 18	160 ± 13	72 ± 14
		$\bar{K}^0 p \to \Sigma^0\pi^+$			
−1.0 to −0.75	16 ± 4	12 ± 3	3.6 ± 0.9	0.61 ± 0.30	$0.55^{+0.51}_{-0.31}$
−0.75 to −0.5	17 ± 5	5.0 ± 1.9			
−0.5 to −0.2	31 ± 6	5.3 ± 1.6	0.95 ± 0.30	<0.092[a]	⋯
−0.2 to 0.2	19 ± 4	9.1 ± 1.9			
0.2 to 0.5	24 ± 5	6.3 ± 1.8			
0.5 to 0.7	29 ± 6	8.6 ± 2.5	3.7 ± 1.2	1.1 ± 0.5	⋯
0.7 to 0.8	26 ± 8	12 ± 4	5.8 ± 2.1	1.3 ± 0.8	⋯
0.8 to 0.9	106 ± 17	32 ± 6	11 ± 2.8	2.8 ± 1.1	⋯
0.9 to 0.95	212 ± 35	114 ± 18	47 ± 8	14 ± 3	$1.1^{+1.6}_{-0.8}$
0.95 to 1.0	245 ± 41	164 ± 22	173 ± 17	132 ± 12	62 ± 13

[a] Corresponds to 1.9 events (85% confidence level) when no events are observed.

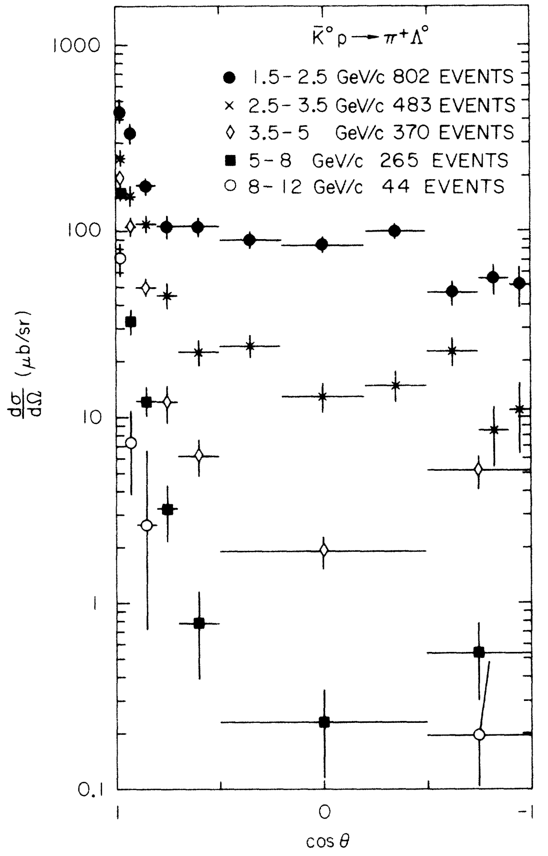

FIG. 10. Differential cross sections versus cosθ in the center-of-mass system for $\bar{K}^0p \to \Lambda\pi^+$.

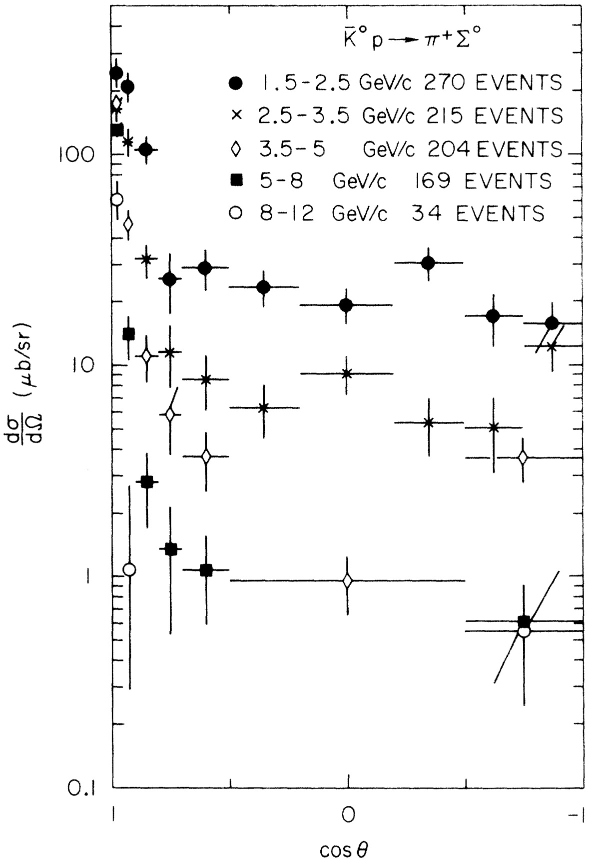

FIG. 11. Differential cross sections versus cosθ in the center-of-mass system for $\bar{K}^0p \to \Sigma^0\pi^+$.

a break in slope near $-t \sim 0.3$ GeV^2 at low momenta, which appears to move out to $-t \sim 0.4 - 0.5$ GeV^2 at higher momenta. The forward peaking, together with the lack of any significant minimum near $-t \sim 0.6$ GeV^2, can be taken as evidence for helicity-nonflip dominance.

Data in the forward region have been parametrized with an exponential form, $d\sigma/dt = Ae^{bt}$, and the results are presented in Table VIII along with the average $t_{\min}$ values for each momentum interval. In the $\Sigma^0\pi^+$ channel the data are consistent with being exponential all the way to $t = 0$, while in the $\Lambda\pi^+$ final state the data in the first t bin ($0.0 \leq -t \leq 0.05$ GeV^2) suggest a turnover or flattening out of the cross section in the forward direction. However, we observe that the parameters obtained when the first bin is excluded or included agree within errors. We note that the $K^-p \to \Lambda\pi^0$ data of Mason and Wohl[19(c)] at 3.13 and 3.30 GeV/c show simple exponential behavior to $t = 0$, while their data at 3.59 GeV/c and the data of Moscoso *et al.*[19(e)] at 3.93 GeV/c exhibit a flattening out in the forward direction; hence, the situation at $t \approx 0$ remains unclear for the $\Lambda\pi$ final state.

The slope parameters from the fits which included the $0.0 \leq -t \leq 0.05$ GeV^2 data are shown in Fig. 14. Superimposed are lines indicating the average slope of previous $K^-N \to \Lambda\pi$ data as well as the nearly momentum-independent slope obtained from $\pi^-p \to \Lambda K^0$ data.[26] Exchange degeneracy demands that the slopes be equal for the π- and $\bar{K}$-induced reactions; yet previous data indicate a 3-standard-deviation separation of the average slope values.[4] Our data, while being consistent with previous K^-N data, suggest shrinkage of the forward slope for the $\bar{K}$ induced reactions, implying possible convergence of the π- and $\bar{K}$-induced reaction slopes near 10 GeV/c.

The situation is quite analogous for the reactions involving a Σ^0. Slopes for the π-induced reactions are large (~ 9 GeV^{-2}) and remain relatively constant with increasing incident momenta,[26] while our data and data on $K^-p \to \Sigma^+\pi^-$ [20] indicate shrinkage of the forward slope for the $\bar{K}$-induced reaction, with possible equality of the π- and $\bar{K}$-induced reaction slopes for $P_{\text{beam}} \gtrsim 6$ GeV/c.

We turn now to the forward cross sections,

TABLE VII. Differential cross sections (in μb/GeV^2).

$-t$ (GeV^2)	Beam momentum interval (GeV/c) 1.5–2.5	2.5–3.5	3.5–5	5–8	8–12
			$\bar{K}^0p \to \Lambda\pi^+$		
0.0–0.05	1813 ± 338	726 ± 139	439 ± 80	229 ± 45	94 ± 57
0.05–0.1	1518 ± 248	735 ± 119	300 ± 56	293 ± 45	123 ± 49
0.1–0.2	931 ± 115	500 ± 63	301 ± 35	151 ± 20	55 ± 17
0.2–0.3	522 ± 84	369 ± 54	174 ± 27	81 ± 15	40 ± 14
0.3–0.4	605 ± 97	241 ± 43	124 ± 23	58 ± 13	14 ± 7
0.4–0.5	642 ± 100	211 ± 40	122 ± 22	16 ± 6	20 ± 13
0.5–0.6	641 ± 100	97 ± 19	58 ± 11	27 ± 6	$2.4^{+2.3}_{-1.4}$
0.6–0.7	377 ± 77				
0.7–1.0	547 ± 57	70 ± 14	29 ± 6	8.4 ± 2.6	
1.0–1.5	479 ± 43	77 ± 12	13 ± 3	4.8 ± 1.7	$1.7^{+2.5}_{-1.2}$
1.5–2.0	307 ± 34	49 ± 9	6.4 ± 2.4	$1.0^{+0.9}_{-0.6}$	
2.0–2.5	179 ± 24	46 ± 10	6.1 ± 2.5	$0.51^{+0.47}_{-0.29}$	...
2.5–3.0	76 ± 15	45 ± 9	$1.1^{+1.7}_{-0.8}$	...	...
			$\bar{K}^0p \to \Sigma^0\pi^+$		
0.0–0.1	1025 ± 154	403 ± 69	393 ± 51	273 ± 35	101 ± 34
0.1–0.2	612 ± 101	315 ± 52	166 ± 27	92 ± 17	48 ± 16
0.2–0.3	266 ± 63	132 ± 32	71 ± 18	46 ± 11	34 ± 17
0.3–0.4	107 ± 48	55 ± 15	30 ± 8	5.7 ± 2.5	$1.7^{+2.5}_{-1.2}$
0.4–0.5	227 ± 65				
0.5–0.7	169 ± 38	34 ± 12	15 ± 6	4.1 ± 1.5	...
0.7–1.0	98 ± 26	29 ± 9	9.0 ± 3.7		
1.0–1.5	122 ± 21	17 ± 6	8.5 ± 2.9	2.1 ± 1.1	...
1.5–2.0	94 ± 21	33 ± 8	4.7 ± 2.1	2.2 ± 1.1	...
2.0–2.5	57 ± 13	18 ± 6	$1.8^{+1.6}_{-1.0}$	...	...
2.5–3.0	12 ± 5	16 ± 6	$2.1^{+1.9}_{-1.2}$	...	...

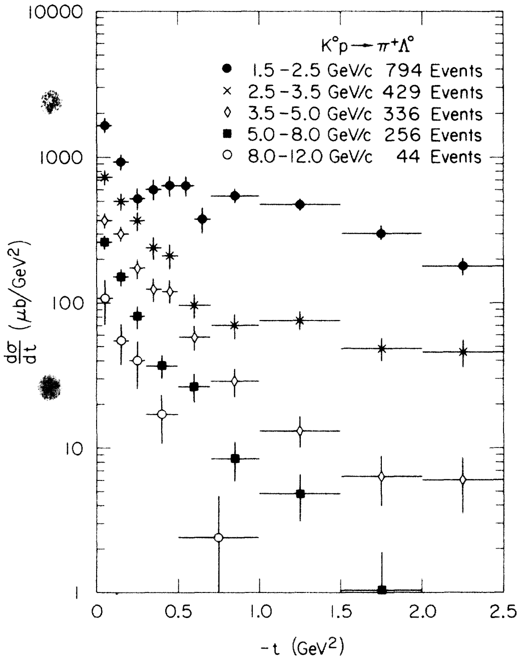

FIG. 12. Differential cross sections versus momentum transfer for $\bar{K}^0p \to \Lambda\pi^+$.

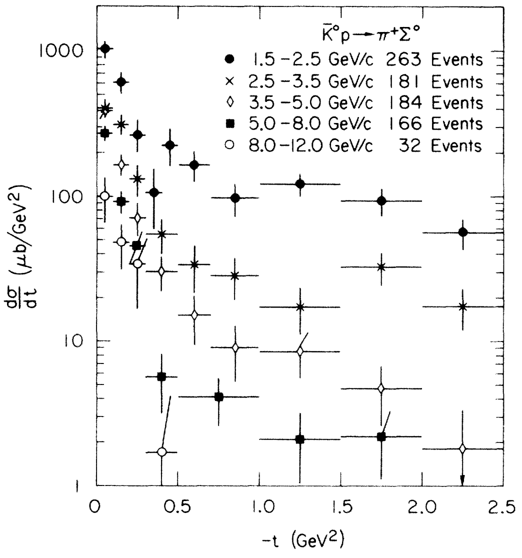

FIG. 13. Differential cross sections versus momentum transfer for $\bar{K}^0p \to \Sigma^0\pi^+$.

TABLE VIII. Forward cross sections fitted to Ae^{bt}. When $\chi^2/NDF > 1$ errors on fitted quantities have been scaled up by the factor $\sqrt{\chi^2/NDF}$.

P_{beam} interval (GeV/c)	$-t$ interval (GeV^2)	A (μb/GeV^2)	b (GeV^{-2})	$\langle t_{\min}\rangle$ (GeV^2)
		$\bar{K}^0p \to \Lambda\pi^+$		
1.5–2.5	0.05–0.3	2470 ± 573	6.6 ± 1.4	0.0175
2.5–3.5	0.05–0.4	935 ± 161	3.9 ± 0.8	0.0127
3.5–5	0.05–0.4	453 ± 79	3.6 ± 0.8	0.0094
5–8	0.05–0.4	395 ± 82	6.2 ± 1.1	0.0064
8–12	0.05–0.4	148 ± 61	6.7 ± 2.1	0.0043
1.5–2.5	0.0–0.3	2235 ± 344	6.0 ± 1.0	0.0175
2.5–3.5	0.0–0.4	868 ± 115	3.6 ± 0.7	0.0127
3.5–5	0.0–0.4	465 ± 62	3.8 ± 0.7	0.0094
5–8	0.0–0.4	303 ± 52	5.0 ± 0.9	0.0064
8–12	0.0–0.4	137 ± 48	6.3 ± 1.9	0.0043
		$\bar{K}^0p \to \Sigma^0\pi^+$		
1.5–2.5	0.0–0.4	1408 ± 228	6.7 ± 1.0	0.0274
2.5–3.5	0.0–0.5	619 ± 101	6.3 ± 0.8	0.0195
3.5–5	0.0–0.5	527 ± 77	7.7 ± 0.9	0.0143
5–8	0.0–0.5	423 ± 66	10.7 ± 1.1	0.0096
8–12	0.0–0.5	131 ± 57	9.2 ± 2.8	0.0064

$(d\sigma/dt)_{t=t_{\min}} = Ae^{bt_{\min}}$, obtained from the parameters of Table VIII. We observe the Σ^0/Λ forward cross-section ratio, R, to rise from 0.73 ± 0.11 for $1.5 \leq P_{\text{beam}} \leq 3.5$ GeV/c to 1.31 ± 0.19 for $3.5 \leq P_{\text{beam}} \leq 12$ GeV/c.[31] If one assumes equality of the vector and tensor amplitudes (octet dominance) and common F/D ratios, it can be shown[9] that

$$R = 3\left(\frac{2F_+ - 1}{2F_+ + 1}\right)^2 ,$$

where F_+ is the helicity-nonflip f-type coupling constant. Solving for F_+ and choosing the solution corresponding to 0° relative phase between the Λ, Σ^0 amplitudes, we obtain

$$F_+ = \frac{1}{2}\left(\frac{1 + (\frac{1}{3}R)^{1/2}}{1 - (\frac{1}{3}R)^{1/2}}\right) .$$

This relation gives $F_+ = 1.47^{+0.15}_{-0.14}$ for $1.5 \leq P_{\text{beam}} \leq 3.5$ GeV/c, in good agreement with the canonical value of $F_+ \approx \frac{3}{2}$.[11] At higher momenta, however,

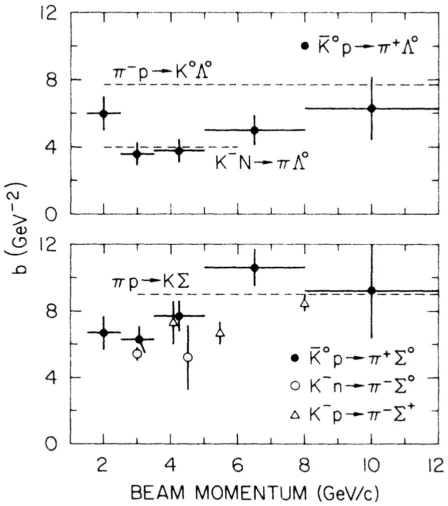

FIG. 14. Forward slopes for $\bar{K}^0p \to \Lambda\pi^+$ (upper figure) and $\bar{K}^0p \to \Sigma^0\pi^+$ (lower figure) versus beam momentum determined in the momentum transfer intervals specified in Table VIII. The dashed lines represent average slope values for the indicated reactions.

TABLE IX. Fit of the data to $s^{2\alpha(t)}/P_{\text{beam}}^2$.

$-t$ interval (GeV^2)	α_{eff}	P_{beam} interval (GeV/c)
	$\bar{K}^0p \to \Lambda\pi^+$	
0.0–0.1	0.24 ± 0.19	3–9
0.1–0.2	0.13 ± 0.22	3–9
0.2–0.3	0.19 ± 0.29	3–9
0.3–0.5	−0.21 ± 0.27	3–9
0.5–0.8	−0.05 ± 0.31	3–9
0.8–1.2	−0.60 ± 0.62	3–7
1.2–2.0	−1.31 ± 0.83	3–6
	$\bar{K}^0p \to \Sigma^0\pi^+$	
0.0–0.1	0.64 ± 0.18	3–10
0.1–0.2	0.35 ± 0.27	3–10
0.2–0.4	−0.08 ± 0.36	3–9
0.4–1.0	−0.60 ± 0.69	3–6

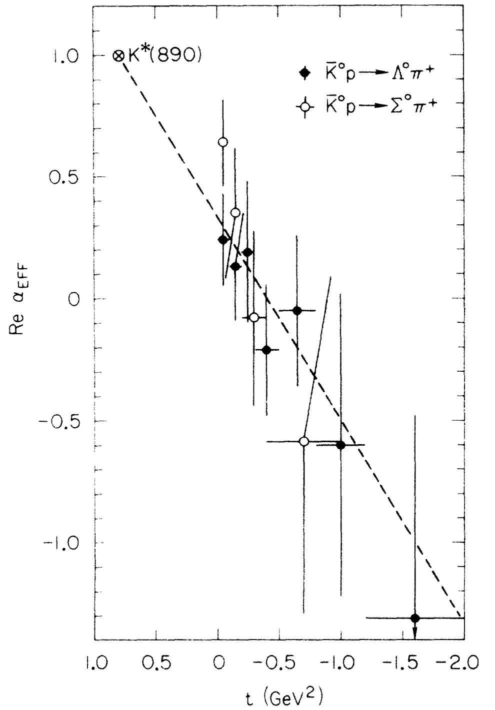

FIG. 15. Real part of the effective Regge trajectory versus momentum transfer for $\bar{K}^0p \to \Lambda\pi^+$ (solid points) and $\bar{K}^0p \to \Sigma^0\pi^+$ (open points). The dashed curve represents the conventional K^* trajectory, $\mathrm{Re}\,\alpha(t) \approx 0.35 + 0.82t$.

we find a larger value of $F_+ = 2.46^{+0.47}_{-0.38}$, which reflects the ~80% rise in R. Only about one-fourth of this increase in R can be accounted for by phase-space and angular-momentum-barrier correction factors.[32] The remainder of this rise may be the result of differences in Λ, Σ^0 final-state interactions.

Finally, to determine the "effective trajectories," the data have also been fitted to the functional form $s^{2\alpha(t)}/{P_{\mathrm{beam}}}^2$. The results are given in Table IX and are shown in Fig. 15. The data in both channels give values of $\alpha(t)$ consistent with the straight-line trajectory, $\mathrm{Re}\,\alpha = 0.35 + 0.82t$, which passes through both K^*'s. However, the $\Sigma^0\pi^+$ data appear to follow a somewhat steeper trajectory.

D. Polarizations

The polarization of the Λ, P_Λ, was determined from the angular distribution of the decay proton with respect to the production normal,[33] $\hat{n} = \hat{q}_i \times \hat{q}_f / |\hat{q}_i \times \hat{q}_f|$, that is,

$$\alpha P_\Lambda = \frac{3}{N} \sum_j^N (\hat{q}_p \cdot \hat{n})_j \ ,$$

where $\alpha = 0.645$ and where $\hat{q}_i$, $\hat{q}_f$, and $\hat{q}_p$ are the momentum unit vectors of the incident meson ($\bar{K}^0$), outgoing meson (π^+), and decay proton, respectively, as seen in the Λ rest frame. The error on αP_Λ is given by $\{[3 - (\alpha P_\Lambda)^2]/N\}^{1/2}$.[34]

POLARIZATION OF Λ^0 IN $\bar{K}^0p \to \pi^+\Lambda^0$

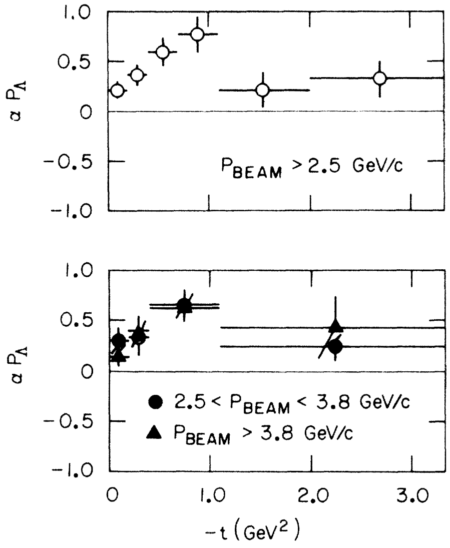

FIG. 16. Polarization of the Λ in $\bar{K}^0p \to \Lambda\pi^+$ versus momentum transfer.

Data on the reaction $\bar{K}^0p \to \Lambda\pi^+$ were divided into two samples, $2.5 < P_{\mathrm{beam}} < 3.8$ GeV/c and $P_{\mathrm{beam}} > 3.8$ GeV/c, with about an equal number of events in each sample. Polarizations obtained from the two samples (Fig. 16, lower) are in good agreement and thus served as justification for combining all data with $P_{\mathrm{beam}} > 2.5$ GeV/c. The data (Table X and Fig. 16, upper) show a large positive Λ polarization, rising rapidly from zero in the forward direction, where it must vanish by angular momentum conservation, peaking near $-t \sim 0.9$ GeV^2, and falling slowly at larger t.

This is in good agreement with the polarization behavior observed in $K^-N \to \Lambda\pi$ data. Comparison with the polarization data from πN experiments[26] shows that for $-t > 0.3$ GeV^2 there is agreement with the EXD prediction of the polarization changing sign under line reversal. However, for $-t < 0.3$ GeV^2 both π and K induced reactions show positive polarization, in violation of the simple EXD hypothesis.

Further justification for combining the polarization data for all beam momenta above 2.5 GeV/c is demonstrated in Fig. 17, which shows the quantity $\langle \alpha P_\Lambda \rangle$, averaged over the momentum transfer interval $0.2 \leqslant -t \leqslant 1.0$ GeV^2,[35] as a function of P_{beam}. The momentum independence of $\langle \alpha P_\Lambda \rangle$, which is also tabulated in Table XI, is clearly evident above the s-channel resonance region ($P_{\mathrm{beam}} \gtrsim 2$ GeV/c).

TABLE X. Hyperon polarization.

$\bar{K}^0p \rightarrow \Lambda\pi^+$

$-t$ (GeV^2)	$\alpha_\Lambda P_\Lambda$ $P_{\mathrm{beam}} > 2.5$ GeV/c	$\alpha_\Lambda P_\Lambda$ $2.5 < P_{\mathrm{beam}} < 3.8$ GeV/c	$\alpha_\Lambda P_\Lambda$ $P_{\mathrm{beam}} > 3.8$ GeV/c
0.0–0.2	0.21 ± 0.08	0.30 ± 0.13	0.15 ± 0.10
0.2–0.4	0.36 ± 0.11	0.32 ± 0.17	0.39 ± 0.15
0.4–0.7	0.59 ± 0.14	0.66 ± 0.15	0.64 ± 0.15
0.7–1.1	0.77 ± 0.18		
1.1–2.0	0.21 ± 0.18	0.23 ± 0.14	0.44 ± 0.32
2.0–3.4	0.32 ± 0.19		

$\bar{K}^0p \rightarrow \Sigma^0\pi^+$

$-t$ (GeV^2)	$\alpha_\Lambda P_\Sigma$ $P_{\mathrm{beam}} > 2.5$ GeV/c
0.0–0.2	-0.18 ± 0.16
0.2–0.4	-0.83 ± 0.32
0.4–1.1	-0.28 ± 0.41
1.1–3.4	-0.06 ± 0.35

From a simple Regge picture the s, t dependence of the polarization would be of the form

$$P(s, t) = G(t)s^{\alpha_2(t)-\alpha_1(t)},$$

where $\alpha_1(t)$ and $\alpha_2(t)$ represent the two highest-lying trajectories exchanged.[30] By identifying these two trajectories with the K^*-K^{**} pair, one might consider the momentum independence of $\langle \alpha P_\Lambda \rangle$ as evidence for weak EXD of the K^*, K^{**} trajectories in the scattering region, $t < 0$.

We have also determined the Σ^0 polarization using the relation

$$\alpha P_\Sigma = -\frac{9}{N} \sum_j^N (\hat{q}_\Lambda \cdot \hat{n})_j (\hat{q}_\Lambda \cdot \hat{k}_p)_j ,$$

where $\hat{q}_\Lambda$ is the momentum vector of the Λ in the Σ^0 rest frame and $\hat{k}_p$ is the proton unit vector in the Λ rest frame.[36] The Σ^0 polarization for data with $P_{\mathrm{beam}} > 2.5$ GeV/c is recorded in Table X. The large errors are the result of poor statistics coupled with the very forward peaking of $d\sigma/dt$.

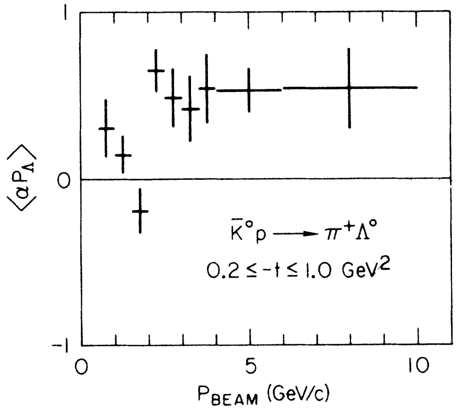

FIG. 17. Polarization of the Λ averaged over the interval $0.2 \leq -t \leq 1.0$ GeV^2 versus incident momentum for the reaction $\bar{K}^0p \rightarrow \Lambda\pi^+$.

IV. DISCUSSION

The sharp forward peaking and the absence of any significant dip structure near $-t \sim 0.6$ GeV^2 in the Λ or Σ^0 differential cross sections (see Figs. 12 and 13) indicates that the s-channel helicity-nonflip amplitude, f_{++}, dominates the $\bar{K}^0p \rightarrow \pi^+(\Lambda, \Sigma^0)$ reactions. A similar result is found for the crossed reactions, $\pi^-p \rightarrow K^0(\Lambda, \Sigma^0)$,[26] confirming that K^*, K^{**} exchanges couple strongly to helicity nonflip at the baryon vertex.

For small values of momentum transfer the modulus of the helicity-nonflip amplitude can be parametrized by a simple exponential

$$f_{++}(t) \sim e^{at},$$

TABLE XI. Average hyperon polarization: $0.2 \leq -t \leq 1.0$ GeV^2.

$\bar{K}^0p \rightarrow \Lambda\pi^+$

P_{beam} (GeV/c)	$\alpha_\Lambda P_\Lambda$
0.5–1.0	0.31 ± 0.17
1.0–1.5	0.15 ± 0.11
1.5–2.0	-0.19 ± 0.14
2.0–2.5	0.65 ± 0.13
2.5–3.0	0.49 ± 0.18
3.0–3.5	0.42 ± 0.20
3.5–4.0	0.54 ± 0.21
4.0–6.0	0.53 ± 0.13
6.0–10.0	0.54 ± 0.24

which then yields an impact-parameter representation of the form

$$f_{++}(b) \sim e^{-b^2/4a}.$$

Alternatively, helicity-flip amplitudes, f_{+-}, have an additional factor of $\sqrt{-t}$ from angular-momentum conservation, and yield

$$f_{+-}(b) \sim b e^{-b^2/4a} .$$

Since absorption depletes the low partial waves (i.e., small b) it is apparent that while helicity-nonflip amplitudes may be strongly modified by absorption, helicity-flip amplitudes are relatively unaffected.[37] Hence, it would not be too surprising if evidence for exchange degeneracy was seriously obscured in hypercharge-exchange reactions, while being easily visible in charge-exchange reactions (involving ρ, A_2 exchanges) which have dominant helicity-flip amplitudes. Thus for hypercharge-exchange reactions, the interpretation of line-reversed reaction pair comparisons may depend heavily on detailed knowledge of the absorption differences in the particular initial and final states.

Unfortunately, conventional absorption models[38] with purely imaginary absorption have proved incapable of providing a qualitative description of the data for two basic reasons. First, evaluation of the absorption for real ($\bar{K}$) versus rotating-phase (π) channels leads to the erroneous prediction that the π-induced cross section should be larger than the $\bar{K}$-induced cross sections. Second, though reasonable polarizations can be predicted for the π-induced reactions, zero polarization results for the $\bar{K}$ channels.

Modified absorption models, such as the dual absorptive model (DAM) of Harari[39] and the Ringland–Roberts–Roy–Tran Thanh Van Reggeized absorption model,[40] are capable of producing respectable fits[12, 41] to the data. However, the former model has little pure predictive power, owing to the unknown real part of the helicity-nonflip amplitude, and the latter provides only a prescription for, not a real understanding of, the absorption procedure. Recently Hartley and Kane,[42] who strive to model in detail the absorption terms, have achieved at least qualitative agreement with essentially all two-body reactions.

Another model, by Field,[43] suggests that lower-lying exchange-degenerate daughter trajectories as well as Pomeron-Regge cuts may be important in the intermediate-energy region, 3–10 GeV/c. This model has the desirable feature of explicitly preserving duality and exchange degeneracy for the bare poles, and isolates the exchange degeneracy and duality breaking to the Pomeron-Regge cut terms. Higher-energy data will provide the true test for this model.

Interestingly, the introduction of phase-space and angular-momentum-barrier corrections[27] may eliminate one of the above-mentioned objections to simple absorption models.[38] One notes that the hyperchange-exchange reactions are always accompanied by a change in masses from initial to final state (e.g., $\pi p \to \Lambda K$ or $\bar{K}p \to \pi\Lambda$). Although such mass shifts appear negligible when compared to incident energies of several GeV, Trilling[27] has suggested that unequal-mass effects can nevertheless be quite large. To compensate for phase-space and angular-momentum-barrier differences, Trilling suggests that cross sections should be scaled by a factor $(p_i/p_f)^{2l+1}$ before making any SU(3) or exchange-degeneracy comparisons. The momenta p_i, p_f are defined in the center-of-mass system and $l = p_i a$ with $a = 0.88$ fm.[27,44] With this correction applied, the resulting $\pi^- p \to K^0(\Lambda, \Sigma^0)$ and $\bar{K}^0 p \to \pi^+(\Lambda, \Sigma^0)$ integrated cross sections are approximately equal, although the uncorrected data differ by factors of ~3.5 at 3 GeV/c and factors of ~1.7 at 10 GeV/c.

From the analysis of the Σ^0/Λ cross section at $t = t_{\min}$ (see Sec. III C and Table VIII) it is observed that the helicity-nonflip coupling constant, F_+, varies substantially with energy (that is, the Σ^0/Λ ratio is not constant). Although there are some problems of relative normalization between different experiments, a compilation of hypercharge-exchange data by Irving, Martin, and Barger[45] also suggests that F_+ is energy dependent. However, recent high-statistics counter experiments yield conflicting results.[26(c),26(e)] Interestingly, the energy dependences of the Λ, Σ^0 data are in agreement at intermediate values of momentum transfer,[45] $-t \sim 0.3$ GeV^2, as shown in Fig. 15. A similar comparison of the energy dependences of $K^0_L p \to K^0_S p$, Kp charge-exchange and $\pi^- p \to \pi^0 n$ data has also observed discrepancies near $t \sim 0$.[46] Absorption or direct-channel effects may provide the simplest explanation of these data.[46]

Although the forward Σ^0, Λ cross sections have a substantial energy dependence in the momentum interval 3 to 10 GeV/c, the Λ-polarization data are observed to be essentially independent of the $\bar{K}^0$ momentum.[47] This result, and the fact that the observed polarizations are large (~80% in $\bar{K}^0 p \to \Lambda\pi^+$ for $0.4 \leq -t \leq 1.1$ GeV^2) provides substantial constraints on t-channel exchange models with low-lying daughter trajectories. Unfortunately, the constraint on the polarization, P, and spin-rotation parameters, R and A,

$$P^2 + A^2 + R^2 = 1 ,$$

then implies that R and A are necessarily small where P is near 1.[10] Thus the R and A parameters for $\bar{K}^0 p \to \pi^+(\Lambda, \Sigma^0)$ may provide only a weak discrimination between various helicity-amplitude structures in the momentum-transfer interval $0.3 \lesssim -t \lesssim 1.0$ GeV^2.

V. SUMMARY AND CONCLUSIONS

We have presented experimental results on the reactions $\bar{K}^0 p \to \Lambda\pi^+$ and $\bar{K}^0 p \to \Sigma^0\pi^+$ from 1 to 12 GeV/c with emphasis placed on the comparison of the Λ and Σ channels and on momentum dependences in the data. The principal features of the data are the following.

(a) The integrated cross sections exhibit power-law, $\sigma \sim P_{\text{beam}}{}^n$, behavior with $n = -2.62 \pm 0.10$ for $1.8 \leqslant P_{\text{beam}} \leqslant 5.0$ GeV/c and $n = -2.21 \pm 0.19$ for $P_{\text{beam}} > 5$ GeV/c in the $\Lambda\pi^+$ channel and with $n = -1.78 \pm 0.09$ for $P_{\text{beam}} \geqslant 1.8$ GeV/c in the $\Sigma^0\pi^+$ channel.

(b) The ratio $\sigma_{\Sigma\pi}/\sigma_{\Lambda\pi}$ in the interval $0.05 \leqslant -t \leqslant 0.4$ GeV^2 is nearly momentum-independent.

(c) The differential cross sections in both reactions exhibit shrinkage of the forward peak, with slope values tending toward the slopes observed in the line-reversed reactions as momentum increases.

(d) The Σ^0/Λ ratio at $t = t_{\text{min}}$ is found to increase with energy. This cannot be explained by simple K^*-K^{**} exchange models, but may suggest that absorption or direct-channel effects are important.

(e) Effective trajectories for both reactions were consistent with a straight line passing through both $K^*(890)$ and $K^{**}(1420)$, except possibly near $t = 0$ in $\Sigma^0\pi^+$ channel.

(f) Hyperon polarization in the $\Lambda\pi^+$ final state is large, positive, and essentially momentum-independent. The polarization averaged over $0.2 \leqslant -t \leqslant 1.0$ GeV^2 varies as $s^{0.15 \pm 0.11}$ for $P_{\text{beam}} \geqslant 2.5$ GeV/c. Σ^0 polarization is found to be large and negative for $0.2 \leqslant -t \leqslant 0.4$ GeV^2.

ACKNOWLEDGMENTS

We thank F. Gilman and R. Cashmore for interesting discussions. We are grateful for the assistance given us by R. Watt and the crew of the SLAC 1-m bubble chamber and by J. Brown and the scanning and measuring staff at SLAC. We also thank D. Johnson for his help with the data reduction.

[†] Work supported by the U. S. Atomic Energy Commission.

[*] Present address: Purdue University, Lafayette, Ind. 47902.

[‡] Present address: Duke University, Durham, N. C. 27706.

[§] Present address: University of Toronto, Toronto, Canada.

[‖] Present address: University of Washington, Seattle, Wash. 98195.

[¶] Present address: National Accelerator Laboratory, Batavia, Ill. 60510.

[**] Present address: Lawrence Berkeley Laboratory, Berkeley, Calif. 94720.

[1] R. C. Arnold, Phys. Rev. Lett. 14, 657 (1965).

[2] D. Cline, J. Matos, and D. D. Reeder, Phys. Rev. Lett. 23, 1318 (1969).

[3] R. D. Matthews, Nucl. Phys. B11, 339 (1969).

[4] K.-W. Lai and J. Louie, Nucl. Phys. B19, 205 (1970).

[5] F. J. Gilman, Phys. Lett. 29B, 673 (1969).

[6] H. Harari, Phys. Rev. Lett. 22, 562 (1969).

[7] J. L. Rosner, Phys. Rev. Lett. 22, 689 (1969).

[8] C. Michael, Nucl. Phys. B13, 644 (1969).

[9] C. Michael and R. Odorico, Phys. Lett. 34B, 422 (1971).

[10] A. C. Irving, A. D. Martin, and C. Michael, Nucl. Phys. B32, 1 (1971).

[11] A. D. Martin, C. Michael, and R. J. N. Phillips, Nucl. Phys. B43, 13 (1972).

[12] J. S. Loos and J. A. J. Matthews, Phys. Rev. D 6, 2463 (1972).

[13] G. W. Brandenburg, A. D. Brody, W. B. Johnson, D. W. G. S. Leith, J. S. Loos, G. J. Luste, J. A. J. Matthews, K. Moriyasu, B. C. Shen, W. M. Smart, F. C. Winkelmann, and R. J. Yamartino, Phys. Rev. D 7, 708 (1973).

[14] Particle Data Group, Rev. Mod. Phys. 45, S1 (1973).

[15] R. J. Yamartino, Ph.D. thesis, Stanford University, 1974 (unpublished).

[16] Zero constraints at the main vertex. The over-all fit still has the three constraints contributed from the secondary vertex.

[17] Events for which (a) $|\hat{\gamma} \cdot \hat{n}| > 0.4$ or (b) $\hat{\gamma} \cdot \hat{\bar{K}}^0 < 0.4$ or (c) $|\hat{\gamma} \cdot \hat{n}| > 0.1$ and $\hat{\gamma} \cdot \hat{\bar{K}}^0 < 0.9$ are assumed to be Σ^0 events.

[18] $K^- n \to \pi^- (\Lambda, \Sigma^0)$: (a) R. Armenteros *et al.*, Nucl. Phys. B18, 425 (1970); (b) SABRE collaboration, Nucl. Phys. B33, 61 (1971); (c) D. J. Crennell *et al.*, Phys. Rev. Lett. 23, 1347 (1969); (d) W. L. Yen *et al.*, Phys. Rev. Lett. 22, 963 (1969); Phys. Rev. 188, 2011 (1969). (e) B. J. Burdick *et al.*, Nucl. Phys. B41, 45 (1972).

[19] $K^- p \to \Lambda\pi^0$: (a) R. Armenteros *et al.*, Nucl. Phys. B8, 233 (1968); (b) SABRE collaboration, Nucl. Phys. B18, 403 (1970); (c) G. C. Mason and C. G. Wohl, Nucl. Phys. B58, 1 (1973); (d) BGLOR collaboration, Phys. Rev. 152, 1148 (1966); Nuovo Cimento 53A, 522 (1968); (e) L. Moscoso *et al.*, Nucl. Phys. B36, 322 (1972); (f) R. Barloutaud, in *Proceedings of the Fourth International Conference on High Energy Collisions, Oxford, 1972*, edited by J. R. Smith (Rutherford High Energy Laboratory, Chilton, Didcot, Berkshire, England, 1972).

[20] $K^- p \to \Sigma^+\pi^-$: (a) A. Berthon *et al.*, Nucl. Phys. B24, 417 (1970); (b) G. W. London *et al.*, Phys. Rev. 143, 1034 (1966); (c) SABRE collaboration, see Ref. 19(b) above; (d) L. Moscoso *et al.*, see Ref. 19(e) above; (e) J. S. Loos *et al.*, Phys. Rev. 173, 1330 (1968); (f) D. Birnbaum *et al.*, Phys. Lett. 31B, 484 (1970); (g) R. Barloutaud, see Ref. 19(f) above.

[21] E. Flaminio *et al.*, CERN/HERA Report No. 70-6, 1970 (unpublished).

[22] E. Bracci *et al.*, CERN/HERA Report No. 72-1, 1972 (unpublished).

[23] $\lambdabar_i$ and $\lambdabar_f$ are the wavelengths ($\lambdabar = \hbar/p$) in the initial and final states, respectively.

[24] D. R. O. Morrison, Phys. Lett. 22, 528 (1966).

[25] A possible exception to the spectral shape insensitivity occurs in the 0.5–1.0-GeV/c bin, where spectral weights differ by a factor of 7 in the space of only 0.5 GeV/c. Coupled with this is the fact that $\Sigma(1620)$ P_{11} and $\Sigma(1664)$ D_{13}, decaying predominantly into $\Sigma\pi$, appear at 630 and 730 MeV/c, while the $\Sigma(1765)$ D_{15}, decaying much more strongly into $\Lambda\pi$, appears at 940 MeV/c near the high-momentum edge of the first bin. Hence, interpretation of the first bin is somewhat dubious and the errors may be underestimated.

[26] $\pi^- p \to K^0(\Lambda, \Sigma^0)$: (a) O. I. Dahl *et al.*, Phys. Rev. 163, 1430 (1967); (b) M. Abramovich *et al.*, Nucl. Phys. B27, 477 (1971); (c) C. E. W. Ward *et al.*, Phys. Rev. Lett. 31, 1149 (1973); (d) D. J. Crennell *et al.*, Phys. Rev. D 6, 1220 (1972); (e) K. J. Foley *et al.*, Phys. Rev. D 8, 27 (1973).

[27] G. H. Trilling, Nucl. Phys. B40, 1 (1972).

[28] G. W. Brandenburg *et al.*, Phys. Lett. 44B, 305 (1973).

[29] The dominance of Δ exchange in backward $\Sigma\pi$ scattering is consistent with $g_{KN\Lambda}^2 \gg g_{KN\Sigma}^2$ [see, for example, G. W. Brandenburg *et al.*, Phys. Rev. Lett. 30, 145 (1973)] and the observation that the $\Lambda\pi$ and $\Sigma\pi$ backward cross sections are approximately equal.

[30] V. D. Barger and D. B. Cline, *Phenomenological Theories of High Energy Scattering* (Benjamin, New York, 1969).

[31] Failure to extrapolate to $t = t_{\text{min}}$ gives somewhat lower $R_{t=0}$ values of 0.67 ± 0.10 for $1.5 \le P_{\text{beam}} \le 3.5$ GeV/c and 1.22 ± 0.18 for $3.5 \le P_{\text{beam}} \le 12$ GeV/c; however, this does not significantly alter our interpretation.

[32] Inclusion of Trilling factors (see text) raises the Σ^0/Λ forward cross-section ratio of 1.06 ± 0.16 and 1.70 ± 0.25, respectively, for the two momentum intervals considered.

[33] E. Segrè, *Nuclei and Particles* (Benjamin, New York, 1964), p. 673.

[34] F. T. Solmitz, Annu. Rev. Nucl. Sci. 14, 375 (1964).

[35] The momentum-transfer limits for the averaging process were chosen mainly with the idea of minimizing $\delta\langle\alpha P_\Lambda\rangle/\langle\alpha P_\Lambda\rangle$, which implies choice of a t region where αP_Λ is large. It is advantageous, therefore, to avoid the abundant supply of low-polarization events at small $-t$ and also to eliminate the nonperipheral contributions at large momentum transfers.

[36] R. Gatto, Phys. Rev. 109, 610 (1958).

[37] B. Sadoulet, Nucl. Phys. B53, 135 (1973).

[38] F. Henyey, G. L. Kane, J. Pumplin, and M. H. Ross, Phys. Rev. 182, 1579 (1969); R. C. Arnold and M. L. Blackmon, *ibid.* 176, 2082 (1968); M. L. Blackmon and G. R. Goldstein, *ibid.* 179, 1480 (1969); C. Michael, Nucl. Phys. B13, 644 (1969).

[39] H. Harari, Ann. Phys. 63, 432 (1971); H. Harari, Stanford Linear Accelerator Center Report No. SLAC-PUB-914 (unpublished); H. Harari, Phys. Rev. Lett. 26, 1400 (1971); 22, 562 (1969).

[40] G. A. Ringland, R. G. Roberts, D. P. Roy, and J. Tran Thanh Van, Nucl. Phys. B44, 395 (1972).

[41] D. Barkai and K. J. M. Moriarty, Nucl. Phys. B50, 354 (1972).

[42] B. J. Hartley and G. L. Kane, Nucl. Phys. B57, 157 (1973).

[43] R. D. Field and J. D. Jackson, Phys. Rev. D 4, 693 (1971); R. D. Field, *ibid.* 5, 86 (1972).

[44] An interaction radius of 0.88 fm corresponds to the first zero of $J_0(a\sqrt{-t})$ occurring at $-t \sim 0.3$ GeV^2.

[45] A. C. Irving, A. D. Martin, and V. Barger, Nuovo Cimento 16A, 573 (1973).

[46] G. W. Brandenburg, W. B. Johnson, D. W. G. S. Leith, J. S. Loos, G. J. Luste, J. A. J. Matthews, K. Moriyasu, W. M. Smart, F. C. Winkelmann, R. J. Yamartino, Phys. Rev. D 9, 1939 (1974).

[47] Actual fits to $\langle\alpha P_\Lambda\rangle \sim s^n$ yield $n = 0.15 \pm 0.11$ for $2.5 \le P_{\text{beam}} \le 10.0$ GeV/c.

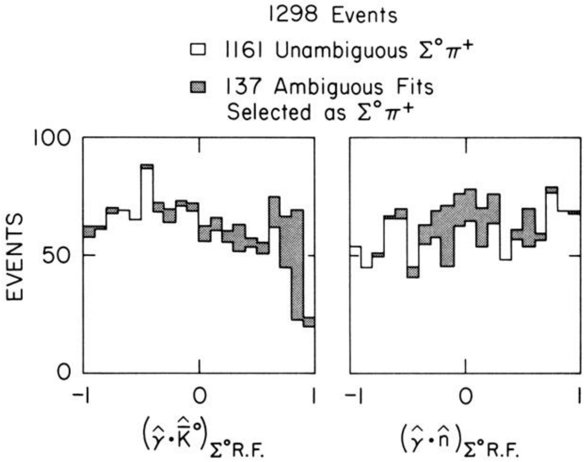

FIG. 4. $\hat{\gamma}\cdot\hat{\hat{K}}^0$ and $\hat{\gamma}\cdot\hat{n}$ distributions for accepted Σ^0 events in the Σ^0 rest frame.

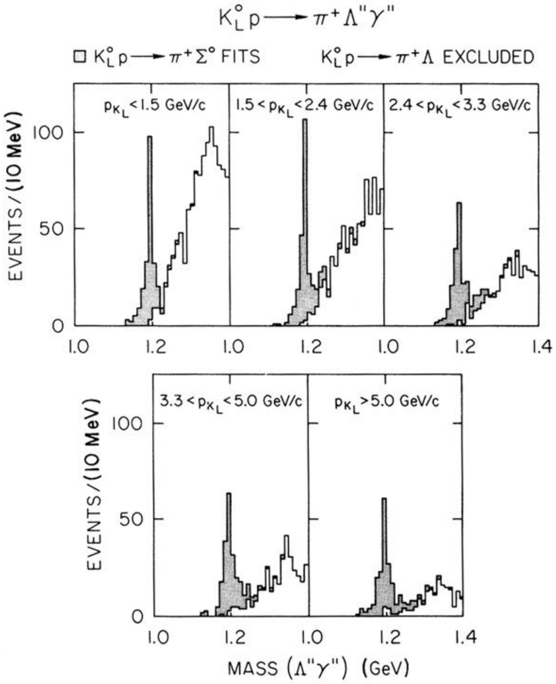

FIG. 5. Invariant mass of the $\Lambda\gamma$ system; $\overline{K}^0 p \rightarrow \Lambda\pi^+$ events are excluded. The shaded events are in the channel $\overline{K}^0 p \rightarrow \Sigma^0\pi^+$.